Renewable and Sustainable Energy Reviews 48 (2015) 857–869

Contents lists available at ScienceDirect

Renewable and Sustainable Energy Reviews

journal homepage: www.elsevier.com/locate/rser

Critical analysis of thermodynamic cycle modeling of adsorption cooling systems for light-duty vehicle air conditioning applications

Amir Sharafian, Majid Bahrami *

Laboratory for Alternative Energy Conversion (LAEC), School of Mechatronic Systems Engineering, Simon Fraser University, # 4300, 250-13450 102nd Avenue, Surrey, BC, Canada V3T 0A3

ARTICLE INFO

Article history:
Received 30 November 2013
Received in revised form
1 February 2015
Accepted 19 April 2015
Available online 22 April 2015

Keywords:
Adsorption cooling system
Vehicle air conditioning
Thermodynamic cycle
Fully dynamic modeling

ABSTRACT

Thermodynamic cycle of adsorption cooling systems (ACS) is thoroughly studied under different operating conditions for light-duty vehicles air conditioning applications. Available ACS prototypes installed in vehicles are discussed in detail followed by different ACS thermodynamic cycle modeling. Also, equilibrium uptake and uptake rate of commonly used working pairs in ACS are summarized. The proper ACS thermodynamic cycle with capability of integration with vehicles' Engine Control Unit (ECU) is developed and it is validated against two sets of experimental data reported in the literature. The realistic input data in agreement with light-duty vehicles are introduced to the model as the base-case condition to produce 2 kW cooling power. Sensitivity of ACS specific cooling power (SCP) and coefficient of performance (COP) are studied with respect to the input parameters. According to the results, the SCP and COP of the base-case ACS are maximized at 10–15 min cycle times and adsorption to desorption time ratio (ADTR) of one. In addition, the results indicate that the adsorber bed overall heat transfer conductance and mass have the highest and the lowest effects on the SCP, respectively. Also, the results show that during the operation of ACS, the heating and cooling fluids, coolant fluid and chilled water mass flow rates do not change the SCP and COP after specific values. As a result, variable speed pumps are required to adjust these mass flow rates to reduce feeding pump powers. Finally, the results indicate that the engine coolant cannot provide enough heat for the adsorber bed desorption process under different operating conditions. Therefore, a portion of the exhaust gas of the engine is recommended to be utilized during the desorption process.

Contents

1. Introduction . . . 858
2. Thermodynamic cycle of ACS . . . 859
3. ACS governing equations . . . 861
   3.1. Mathematical modeling . . . 861
   3.2. Working pairs' characteristics . . . 861
   3.3. Solution method . . . 862
4. Results and discussion . . . 863
   4.1. Comparison of the model against the experimental data . . . 863
   4.2. Base-case model . . . 864
   4.3. Parametric study . . . 864
5. Conclusion . . . 867
Acknowledgment . . . 867
References . . . 867

* Corresponding author. Tel.: +1 778 782 8538; fax: +1 778 782 7514.
E-mail addresses: asharafi@sfu.ca (A. Sharafian), mbahrami@sfu.ca (M. Bahrami).

http://dx.doi.org/10.1016/j.rser.2015.04.055
1364-0321/

Nomenclature

A	heat transfer surface area (m^2)
A/C-R	air conditioning and refrigeration
ACS	adsorption cooling system
$ADTR$	adsorption to desorption time ratio
a_i	constants
b_i	constants
c	heat capacity of solid materials (J/kg K)
c_p	heat capacity at constant pressure (J/kg K)
COP	coefficient of performance
D_s	solid-side mass diffusivity (m^2/s)
D_{s0}	pre-exponential constant (m^2/s)
E_a	activation energy (J/mol)
Δh_{ads}	enthalpy of adsorption (J/kg)
ΔT_{LM}	log mean temperature difference (K)
HTS	heat transfer fluid
h_{fg}	enthalpy of vaporization (J/kg)
ICE	internal combustion engine
M	molar mass (kg/mol)
m	mass (kg)
$\dot{m}$	mass flow rate (kg/s)
P	pressure (mbar)
Q_{total}	total heat transfer (J)
$\dot{q}$	heat transfer rate (W)
R_p	average radius of adsorbent particles (m)
R_u	universal gas constant (J/mol K)
SCP	specific cooling power (W/kg dry adsorbent)
ω	adsorbate uptake (kg/kg dry adsorbent)
T	temperature (K)
t	time (s)
τ_{cycle}	cycle time (s)
U	overall heat transfer coefficient (W/m^2 K)
$VCRC$	vapor compression refrigeration cycle

Subscripts

adsorbate	adsorbate
adsorbent	adsorbent particles
bed	adsorber bed
chilled	chilled water
cf	cooling fluid
cond	condenser
coolant	coolant fluid
cooling	cooling process
eq	equilibrium state
evap	evaporator
heating	heating process
hf	heating fluid
i	in
liq.	liquid phase
max	maximum
min	minimum
o	out
sat	saturation
vaporous	vaporous phase

1. Introduction

Vapor compression refrigeration cycles (VCRC) are the most popular air conditioning and refrigeration (A/C-R) systems used in residential and industrial buildings, chemical and process engineering, and the automotive sector. Annually, A/C systems of light duty vehicles in the US consume about 40 billion liters of fuel [1]. To maintain the cabin temperature within the acceptable thermal comfort temperature range, 20–23 °C [2], a compressor of VCRC installed in a typical medium size sedan consumes up to 5–6 kW of the power that the internal combustion engines (ICE) generates. This power is equivalent to the required power for a 1200-kg sedan cruising at 56 km/h [1]. Moreover, approximately 70% of the total fuel energy released in the ICE is wasted through the engine coolant and exhaust gases [3]. A prominent replacement of VCRC is adsorption cooling systems (ACS) in which adsorber beds replace the compressor. ACS take advantage of sorption phenomenon in which a fluid (adsorbate) is adsorbed at the surface of a porous solid material (adsorbent). Common working adsorption pairs used in ACS include: zeolite–water, silica gel–water and activated carbon–methanol. Most of these materials are environmentally friendly, non-toxic, non-corrosive, and inexpensive [4]. Moreover, ACS are quiet and easy to maintain because they do not have any moving parts, except valves [5]. Thus, ACS are ideal candidates for applications where waste-heat or low-grade thermal energy (~100 °C) is available. However, commercialization of ACS faces major challenges; namely: (i) low specific cooling power (SCP), (ii) low coefficient of performance (COP), and (iii) high adsorber bed to adsorbent mass ratio which result in heavy and bulky system. The focus of this study is on light-duty vehicle applications and the following provides the pertinent literature to ACS designed and built for vehicles A/C-R applications.

In 1929, Hulse [6] built the first commercial silica gel–sulphur dioxide ACS and installed it in a freight car refrigeration system to carry fish and meat all over the US. The designed system was able to keep the freezer room temperature as low as −12 °C with minimum moving and control parts, and has the capability of working at car idle time. This ACS consisted of two adsorber beds, an air-cooled condenser and two gas burners to supply high temperature gas for the desorption process. With the advent of compressors and emergence of VCRC, ACS were forgotten for several decades; however, due to VCRC high energy consumption, negative environmental impacts and stringent government emission regulations, ACS have been reconsidered from 1990s. Feasibility of VCRC replacement with ACS in electric vehicles (EVs) was analytically investigated by Aceves [7]. According to his calculations, during a 60 min driving cycle, the A/C system should be able to bring the cabin temperature down from the hot soak (43 °C) to the comfort (25 °C and 60% relative humidity) conditions within the first 15 min. As a result, Aceves' calculations showed that the maximum required cooling power is 2 kW and to keep the cabin temperature constant, the A/C system should continuously supply 1.5 kW cooling power. Finally, Aceves concluded that the mass of VCRC could be up to 20% lighter than that of ACS. It should be noted that, in Aceves' analysis, the COP of 2.2 was assumed for the vehicles' VCRC; however, the COP of vehicles' VCRC is between 1.0–1.6 in real applications [8–10]. Suzuki [3] assessed the possibility of using the ACS for automobile A/C applications and studied the effects of adsorber bed overall heat transfer conductance, UA (W/K), on the SCP of zeolite–water ACS. Suzuki reported that the engine coolant at the inlet of the radiator and the engine exhaust gas at the outlet of the piston compartment were at 95 °C and 400–600 °C, respectively; and these temperatures were enough for regeneration of the adsorber beds. Suzuki, also, mentioned that the power generated in a compact vehicle with a 2000 cc ICE were about 10.8 and 35–50 kW at the idle and city driving (60 km/h) conditions, respectively [3]. As such, one can conclude that the

amount of heat dissipated through the engine coolant and the ICE exhaust gas during the idle and city driving conditions are equal to 7.5 and 24.5–35 kW, which is equivalent to 70% of fuel released energy. Accordingly, the COP of an ACS with 2 kW cooling power should be at least 0.27 (=2 kW (max. cooling load)/7.5 kW (available waste heat at the idle condition)) and 0.057 (=2 kW (max. cooling load)/35 kW (available waste heat at the city driving condition)). Thus, one can conclude that: (i) the COP of ACS is not important in vehicle applications where the ICE waste-heat is utilized, and (ii) a fraction of the ICE waste heat suffices to run an ACS to meet the A/C needs of a vehicle. As such, our focus in this study will be on the SCP and adsorber bed to adsorbent mass ratio of ACS for vehicle applications.

Zhang et al. [11–15] proposed non-equilibrium lumped-body and 3D numerical models for a two-adsorber bed, zeolite–water ACS for automobile waste heat recovery. They studied the effects of different parameters such as heat transfer fluid (HTF) inlet temperature, evaporation and condensation temperatures, cycle time, and overall heat transfer conductance on the SCP and COP of ACS. They concluded that the SCP is more sensitive to the variation of operating conditions, namely, evaporation, condensation and regeneration temperatures, than the COP. In both Suzuki's [3] and Zhang's [11–15] models, the evaporator and condenser physical properties were not included in the modeling and it was assumed that the evaporator and condenser are perfect heat exchangers with infinite overall heat transfer conductance.

Jiangzhou et al. [16] and Lu et al. [17] built a locomotive waste heat driven, single-adsorber bed, zeolite 13X-water ACS to produce 4 kW cooling power with a SCP and COP of 19 W/kg dry adsorbent and 0.25, respectively. In their system, 140 kg of zeolite was packed in a 260-kg steel adsorber bed with 10–12 W/m^2 K overall heat transfer coefficient; the low overall heat transfer coefficient resulted in a low heat transfer rate and, consequently, low SCP of 19 W/kg dry adsorbent. Christy and Toossi [18] studied the feasibility of installing a four-adsorber bed, activated carbon-ammonia ACS on containerships and heavy-duty vehicles. Their analysis showed that to drive a compressor of refrigerated trailers, a 25-kW auxiliary diesel engine annually consumed about 4500–6000 l of diesel fuel and emitted 29 kg of carbon monoxide if the A/C system only worked during 50% of the duty cycle. In their adsorber bed design, they determined that if the waste heat is directly supplied from the exhaust pipe, the maximum allowable backpressure on the exhaust gas along the exhaust line should be less than 10 kPa. To prevent increasing the backpressure, the inner diameter of HTF line inside the adsorber bed should be between 12.7 and 15.24 cm (5–6 in.) [18]. Also, they tried to build a prototype ACS; however, their system failed due to ammonia leakage.

Lambert and Jones [19,20] studied the viability of using ACS for automotive A/C applications and proposed a conceptual design for an activated carbon–ammonia ACS. To reduce the backpressure on the exhaust gas line, they suggested using a phase-change material (PCM) heat storage tank to transfer heat from the exhaust gas to HTF and storing heat for running the ACS after shutting off the engine. Wang et al. [21–25] designed a two-adsorber bed, consolidated activated carbon/$CaCl_2$–ammonia ACS to produce ice in fishing boats. The exhaust gas of the boats' diesel engine was utilized to regenerate the adsorbent particles and to prevent corrosion of the adsorber beds and condenser in contact with the salt water, Wang et al. [21–25] proposed using heat pipes. The added heat pipes increased the ACS performance, however, the overall mass of the system also increased. Therefore, using heat pipes is not recommended for light-duty vehicles' A/C applications. De Boer et al. [2,26] built and installed a two-adsorber bed, silica gel–water ACS with 2-kW cooling power for the first time in a compact car, Fiat Stilo. Their analysis showed that the engine coolant was sufficient to meet the A/C needs of the cabin if the COP of ACS was greater than 0.5. However, in the final product, they added a heat exchanger to use the ICE exhaust gas as well. In their setup, each adsorber bed was filled with about 3 kg of silica gel and the adsorber bed to adsorbent mass ratio was 4.2 which indicated that each adsorber bed was 12.6 kg. The 86 kg total mass of their system greatly exceeded the 35 kg limit set by the car manufacturer [2].

Narayanan et al. [27,28] recently proposed the idea of an adsorption-based thermal battery for EVs' A/C application. The 2-kWh single-adsorber bed thermal battery was regenerated by electric heaters when the EV's batteries were being charged to produce cooling power for the on-duty vehicle. However, Narayanan et al. [27,28] did not discuss about the total weight of the thermal battery and its advantages instead of adding extra Li-ion battery packs for running the conventional VCRC. One can conclude from the literature review that bulkiness and weight of the current designs are the main challenges facing the commercialization of ACS.

Developing an accurate thermodynamic model that includes the heat and mass transfer phenomena in the adsorber bed, evaporator and condenser, and accurately predicts the behavior of ACS under various operating conditions is the first step toward designing a mobile ACS with optimum footprint and weight. The proposed model should provide (i) high convergence rate to find the optimized operating conditions of the system within a short time, and (ii) possibility of integrating with the vehicles' Engine Control Unit (ECU). In this paper, different thermodynamic models are compared against each other and required information about different working pairs is summarized. The nominated thermodynamic model is verified against two sets of experimental data available in the literature and, finally, effects of different parameters are studied on the SCP and COP of silica gel–water ACS for light-duty vehicle A/C applications.

2. Thermodynamic cycle of ACS

An ACS works based on two main processes: heating–desorption–condensation and cooling–adsorption–evaporation. When repeating

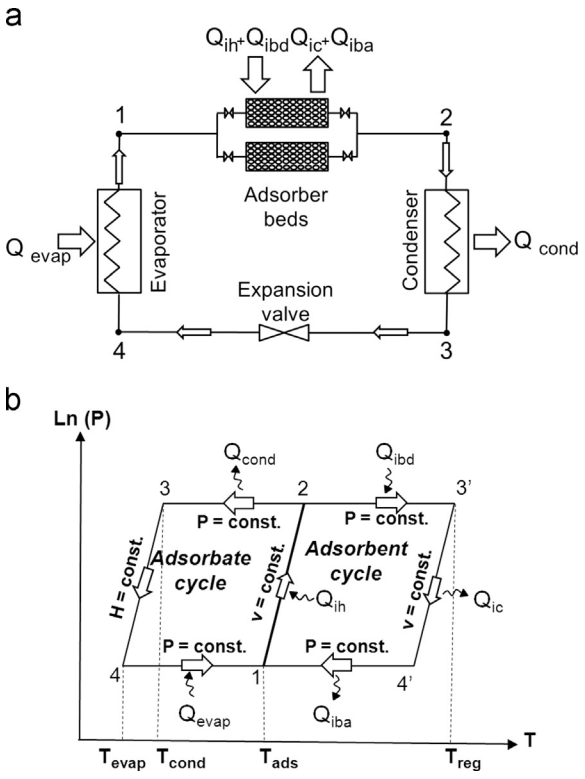

Fig. 1. (a) Schematic of main parts in a waste heat-driven two-adsorber bed ACS, and (b) thermodynamic processes in an ACS [29].

these processes, ACS produces intermittent evaporative cooling power during each cycle. To produce continuous cooling power, more than one adsorber bed can be used. Fig. 1a depicts a typical ACS including adsorber beds, condenser, expansion valve, and evaporator. As shown in Fig. 1a, the ACS is similar to a VCRC, except that the adsorber beds replace the compressor.

Fig. 1b shows the thermodynamic cycle of an ACS which is divided into two subcycles: (i) adsorbent cycle (on the right-side), and (ii) adsorbate cycle (on the left-side). As shown in Fig. 1b, thermodynamic processes in the adsorbent cycle are: (1) isosteric heating (ih); process 1-2, (2) isobaric desorption (ibd); process 2-3′, (3) Isosteric cooling (ic); process 3′-4′, and (4) isobaric adsorption (iba); process 4′-1. Isosteric and isobaric processes refer to constant specific volume and pressure processes, respectively.

During step 1-2, adsorbent–adsorbate pair through an isosteric process absorbs heat in amount of Q_{ih} from an external heat source. In this step, temperature and pressure of the adsorber bed increase due to the adsorbate desorption from the adsorbent particles. This process is continued until the pressure of the adsorber bed reaches the pressure of the condenser. At this time, the inlet valve to the condenser is opened. In step 2-3′, the external heat source continuously heats the adsorber bed (Q_{ibd}) during an isobaric desorption process and the adsorbate leaves the adsorber bed and is condensed inside the condenser during an isobaric cooling process (step 2-3). After heating the adsorber bed up to the point 3′ which is the maximum temperature of the cycle, the valve between the adsorber bed and the condenser is closed and during an isosteric cooling process (step 3′-4′), the adsorbent loses its heat (Q_{ic}) in contact with a heat sink. In step 3-4, the adsorbate inside the condenser passes through the expansion valve and enters to the evaporator. During step 4-1, the adsorbate absorbs heat in amount of Q_{evap} from the environment of interest and converts to the vapor. At the same time, the entrance valve to the adsorber bed is opened and the adsorbent adsorbs the vapor adsorbate during an isobaric adsorption process (step 4′-1) and releases its heat (Q_{ibd}).

To simulate the ACS thermodynamic cycle, different assumptions and simulations have been reported in the literature. Yong and Sumathy [30] reviewed and categorized the available mathematical models in the ACS thermodynamic cycle modeling. However, there is no conclusive evidence on what model is superior. We categorized the mathematical models into three main groups: (i) analytical models, (ii) lumped-body models, and (iii) geometry-dependent models. Analytical models are the simplest and fastest method in design and analysis of ACS performance. In these models, the first law of thermodynamics is used to analytically evaluate the SCP and COP of ACS such as models reported by Aceves [7], Christy and Toossi [18] and Lambert and Jones [19,20]. The analytical models cannot predict the cycle time and the status each process. To solve these limitations, lumped-body models were proposed. These models are a combination of the first law of thermodynamics and mass transfer equations. They consist of ordinary differential equations to increase the accuracy of the model and can predict the cycle time, SCP, and the ACS status during each process. Geometry-dependent models are a combination of heat and mass transfer equations, and spatial parameters. The governing equations are mainly partial differential equations and the finite element, finite volume and finite difference methods are used to discretize and solve the set of equations. Further information about geometry-dependent models can be found elsewhere, e.g. [12,15,31–42]. Although these models are suitable to study the heat and mass transfers through the adsorber bed in detail, the computing time and complexity of analysis do not permit the integration of these models with the on-duty vehicle A/C system. In this study, we focus on lumped-body models to find a reliable model with short computing time. To this end, we classified ACS lumped-body models into three subgroups as summarized in Table 1.

As shown in Table 1, quasi-steady state models have some limitations and cannot predict the cycle time and SCP of ACS. The ACS dynamic modeling with perfect condenser and evaporator are more flexible; however, they cannot estimate the effects of condenser and evaporator on the COP and SCP of ACS. Also, Restuccia et al. [63] experimentally showed that the condenser and evaporator pressures are not constant during the desorption and adsorption processes (processes 2-3′ and 4′-1 in Fig. 1b) because the condenser and evaporator pressures vary with the adsorbate flow rate, for example the condenser pressure is higher at the start of the desorption process than the end of the desorption process. Therefore, the ACS dynamic modeling with perfect condenser and evaporator is not a complete model and should be modified. To

Table 1
Different ACS lumped-body models reported in the literature.

ACS lumped-body models	Governing equations	Advantages	Limitations	Used by
Quasi-steady state	• 1st law of thermodynamics • Equilibrium adsorbate uptake	• Quick method • Estimates maximum evaporative cooling energy and COP	• Time-independent • Cannot predict the cycle time and SCP	• Cacciola and Restuccia [43] • Hajji and Khalloufi [44] • Sharafian and Bahrami [29]
Dynamic modeling with perfect condenser and evaporator	• 1st law of thermodynamics • Equilibrium adsorbate uptake • Adsorbate uptake rate	• Predicts adsorbate uptake rate, cycle time, COP, and SCP • Captures trend of experimental data • High convergence rate	• Perfect condenser and evaporator with infinite heat transfer conductance • Constant condenser and evaporator pressures • Overestimating the results	• Sakoda and Suzuki [45,46] • Tiansuwan et al. [47] • Saha et al. [48,49] • Wu et al. [50]
Fully dynamic modeling	• 1st law of thermodynamics • Equilibrium adsorbate uptake • Adsorbate uptake rate • Condenser and evaporator heat transfer equations	• Predicts adsorbate uptake rate, cycle time, COP, and SCP • Variable condenser and evaporator pressures • High convergence rate • Good accuracy	• Requires a large number of inputs to the model	• Chua et al. [51] • Ref. [52–62]

solve these limitations, ACS fully dynamic thermodynamic cycle is proposed.

3. ACS governing equations

In this section, governing equations for an ACS fully dynamic model are developed. In addition, different working pairs' characteristics were included in this modeling to develop a comprehensive model for the ACS sizing and rating under different operating conditions.

3.1. Mathematical modeling

The governing equations of the ACS fully dynamic thermodynamic cycle are summarized in Table 2.

To find the adsorbent particles temperature, adsorbate uptake rate, and heating fluid and condenser coolant outlet temperatures during the isosteric heating and isobaric desorption processes, Eqs. (1)–(3) and Eqs. (2)–(8) should be solved simultaneously. Similarly, Eqs. (11)–(13), and Eq. (5) and Eqs. (12)–(17) should be solved simultaneously during the isosteric cooling and isobaric adsorption processes. The total amount of heat transfer to/removal from the adsorber beds, condenser and evaporator are calculated from Eqs. (20)–(23), and the COP and SCP of ACS are determined using Eqs. (24) and (25), respectively.

3.2. Working pairs' characteristics

Silica gel–water, activated carbon–methanol, activated carbon–ethanol, and zeolite–water are conventional working pairs in ACS. To increase the adsorbate uptake rate in ACS, a wide range of composite adsorbent materials have been developed recently; however, limited information about the adsorbate uptake rate has been reported in the literature which is an important parameter in ACS thermodynamic cycle modeling. In this section, performance parameters and thermo-physical properties are presented for well-

Table 2
Governing equations on ACS fully dynamic thermodynamic cycle modeling.

Process in Fig. 1b	Governing equation (Eq. no.)
Isosteric heating (Step 1-2)	$m_{adsorbent}\left[c_{adsorbent}+c_{p,liq.\ \ adsorbate}\omega_{max}+c_{bed}\frac{m_{bed}}{m_{adsorbent}}\right]\frac{dT_{adsorbent}}{dt}=U_{bed}A_{bed}\Delta T_{LM,bed}$ (1)
	$\Delta T_{LM,bed}=\frac{T_{hf,i}-T_{hf,o}}{\ln\left(\frac{T_{hf,i}-T_{adsorbent}}{T_{hf,o}-T_{adsorbent}}\right)}$ (2)
	$\dot{m}_{hf}c_{p,hf}\left(T_{hf,i}-T_{hf,o}\right)=U_{bed}A_{bed}\Delta T_{LM,bed}$ (3)
Isobaric desorption (Step 2-3')	$m_{adsorbent}\left[c_{adsorbent}+c_{p,liq.\ \ adsorbate}\omega+c_{bed}\frac{m_{bed}}{m_{adsorbent}}\right]\frac{dT_{adsorbent}}{dt}-m_{adsorbent}\frac{d\omega}{dt}\Delta h_{ads}$ $=U_{bed}A_{bed}\Delta T_{LM,bed}$ (4)
	$\frac{d\omega}{dt}=\frac{15D_s}{R_p^2}(\omega_{eq}-\omega)=\frac{15D_{s0}}{R_p^2}\exp\left(-\frac{E_a}{R_uT_{adsorbent}}\right)(\omega_{eq}-\omega)=k_1\exp(-\frac{k_2}{T_{adsorbent}})(\omega_{eq}-\omega)$ (5)
Condensation (Step 2-3)	$-m_{adsorbent}\frac{d\omega}{dt}\left[h_{fg,\ adsorbate\ @\ T_{cond}}+c_{p,vaporous\ adsorbate}(T_{adsorbent}-T_{cond})\right]-U_{cond}A_{cond}\Delta T_{LM,cond}$ $=m_{cond}c_{cond}\frac{dT_{cond}}{dt}$ (6)
	$\Delta T_{LM,cond}=\frac{T_{coolant,i}-T_{coolant,o}}{\ln\left(\frac{T_{cond}-T_{coolant,o}}{T_{cond}-T_{coolant,i}}\right)}$ (7)
	$\dot{m}_{coolant}c_{p,coolant}\left(T_{coolant,o}-T_{coolant,i}\right)=U_{cond}A_{cond}\Delta T_{LM,cond}$ (8)
Heating and condensation heat transfer rates	$\dot{q}_{heating}=\dot{m}_{hf}c_{p,hf}\left(T_{hf,i}-T_{hf,o}\right)$ (9)
	$\dot{q}_{cond}=\dot{m}_{coolant}c_{p,coolant}\left(T_{coolant,i}-T_{coolant,o}\right)$ (10)
Isosteric cooling (Step 3'-4')	$m_{adsorbent}\left[c_{adsorbent}+c_{p,liq.\ \ adsorbate}\omega_{min}+c_{bed}\frac{m_{bed}}{m_{adsorbent}}\right]\frac{dT_{adsorbent}}{dt}=U_{bed}A_{bed}\Delta T_{LM,bed}$ (11)
	$\Delta T_{LM,bed}=\frac{T_{cf,i}-T_{cf,o}}{\ln\left(\frac{T_{cf,i}-T_{adsorbent}}{T_{cf,o}-T_{adsorbent}}\right)}$ (12)
	$\dot{m}_{cf}c_{p,cf}\left(T_{cf,i}-T_{cf,o}\right)=U_{bed}A_{bed}\Delta T_{LM,bed}$ (13)
Isobaric adsorption (Step 4'-1)	$m_{adsorbent}\left[c_{adsorbent}+c_{p,liq.\ \ adsorbate}\omega+c_{bed}\frac{m_{bed}}{m_{adsorbent}}\right]\frac{dT_{adsorbent}}{dt}-$ $m_{adsorbent}\frac{d\omega}{dt}\left[\Delta h_{ads}-c_{p,vaporous\ adsorbate}\left(T_{adsorbent}-T_{evap}\right)\right]$ $=U_{bed}A_{bed}\Delta T_{LM,bed}$ (14)
Evaporation (Step 4-1)	$-m_{adsorbent}\frac{d\omega}{dt}\left[h_{fg,\ adsorbate\ @\ T_{evap}}-c_{p,liq.\ adsorbate}\left(T_{cond}-T_{evap}\right)\right]+U_{evap}A_{evap}\Delta T_{LM,evap}$ $=m_{evap}c_{evap}\frac{dT_{evap}}{dt}$ (15)
	$\Delta T_{LM,evap}=\frac{T_{chilled,i}-T_{chilled,o}}{\ln\left(\frac{T_{chilled,i}-T_{evap}}{T_{chilled,o}-T_{evap}}\right)}$ (16)
	$\dot{m}_{chilled}c_{p,chilled}\left(T_{chilled,i}-T_{chilled,o}\right)=U_{evap}A_{evap}\Delta T_{LM,evap}$ (17)
Cooling and evaporation heat transfer rates	$\dot{q}_{cooling}=\dot{m}_{cf}c_{p,cf}\left(T_{cf,i}-T_{cf,o}\right)$ (18)
	$\dot{q}_{evap}=\dot{m}_{chilled}c_{p,chilled}\left(T_{chilled,i}-T_{chilled,o}\right)$ (19)
Total heat transfer to adsorber beds, condenser and evaporator	$Q_{total\ \ heating}=\int_{steps\ (1-2)+(2-3')}\dot{q}_{heating}\ dt(J)$ (20)
	$Q_{total\ \ cooling}=\int_{steps\ (3'-4')+(4'-1)}\dot{q}_{cooling}\ dt(J)$ (21)
	$Q_{cond}=\int_{step\ (2-3)}\dot{q}_{cond}\ dt(J)$ (22)
	$Q_{evap}=\int_{step\ (4-1)}\dot{q}_{evap}\ dt(J)$ (23)
Performance of ACS	$COP=\frac{Q_{evap}}{Q_{total\ \ heating}}$ (24)
	$SCP=\frac{Q_{evap}}{m_{adsorbent}\tau_{cycle}}(W/\mathrm{kg})$ (25)

Table 3
Equilibrium adsorbate uptake and enthalpy of adsorption of different working pairs in ACS.

Working pair	Equilibrium equation	Enthalpy of adsorption (J/kg)	Constant parameters	Ref. no.
Zeolite 4A–water	$\ln(P)=a(\omega)+\frac{b(\omega)}{T_{adsorbent}}$, P in mbar, T in K $a(\omega)=a_0+a_1\omega+a_2\omega^2+a_3\omega^3$ $b(\omega)=b_0+b_1\omega+b_2\omega^2+b_3\omega^3$	$\Delta h_{ads}=\frac{R_u}{M_{adsorbate}}b(\omega)$	$a_0=14.8979$, $b_0=-7698.85$ $a_1=95.408$, $b_1=21498.1$ $a_2=-636.66$, $b_2=-184598.0$ $a_3=1848.8$, $b_3=512605.0$ $R_u=8.314$ J/mol K $M_{adsorbate}=0.018$ kg/mol	[43]
Zeolite 13X–water	$\ln(P)=a(\omega)+\frac{b(\omega)}{T_{adsorbent}}$, P in mbar, T in K $a(\omega)=a_0+a_1\omega+a_2\omega^2+a_3\omega^3$ $b(\omega)=b_0+b_1\omega+b_2\omega^2+b_3\omega^3$	$\Delta h_{ads}=\frac{R_u}{M_{adsorbate}}b(\omega)$	$a_0=13.4244$, $b_0=-7373.78$ $a_1=110.854$, $b_1=6722.92$ $a_2=-731.76$, $b_2=5624.47$ $a_3=1644.8$, $b_3=-3486.7$ $R_u=8.314$ J/mol K $M_{adsorbate}=0.018$ kg/mol	[43]
Act. carbon–methanol	$\ln(P)=a(\omega)+\frac{b(\omega)}{T_{adsorbent}}$, P in mbar, T in K $a(\omega)=a_0+a_1\omega+a_2\omega^2+a_3\omega^3$ $b(\omega)=b_0+b_1\omega+b_2\omega^2+b_3\omega^3$	$\Delta h_{ads}=\frac{R_u}{M_{adsorbate}}b(\omega)$	$a_0=20.3305$, $b_0=-6003.58$ $a_1=6.53035$, $b_1=6315.16$ $a_2=-16.6841$, $b_2=-26058.7$ $a_3=52.3793$, $b_3=40537.9$ $R_u=8.314$ J/mol K $M_{adsorbate}=0.032$ kg/mol	[43]
Act. carbon–ethanol	$\omega_{eq}=\omega_0\exp\left[-A\left[T_{adsorbent}\ln\left(\frac{P_{sat\ @\ T_{adsorbent}}}{P_{cond\ or\ evap}}\right)\right]^2\right]$, T in K	$\frac{\Delta h_{ads}-h_{fg}}{E}=\left[\ln\left(\frac{\omega_0}{\omega_{eq}}\right)\right]^{1/n}+a\left[\frac{T_{adsorbent}}{T_c}\right]^b$	$\omega_0=0.797$ kg/kg $A=1.716\times10^{-6}$ K^{-2} $a=6.717$, $b=9.75$ $n=2$, $E=138$ kJ/kg $T_c=789.15$ K	[64]
RD silica gel–water	$\omega_{eq}=\frac{K_0\exp\left(\frac{\Delta h_{ads}M_{adsorbate}}{R_uT_{adsorbent}}\right)P}{\left[1+\left[\frac{K_0}{\omega_m}\exp\left(\frac{\Delta h_{ads}M_{adsorbate}}{R_uT_{adsorbent}}\right)P\right]^n\right]^{1/n}}$, P in *mbar*, T in *K*	$\Delta h_{ads}=2693$ kJ/kg	$K_0=7.3\times10^{-11}$ mbar^{-1} $\omega_m=0.45$ kg/kg $n=12$ $R_u=8.314$ J/mol K $M_{adsorbate}=0.018$ *kg/mol*	[65]
Silica gel/$CaCl_2$–water	$\omega_{eq}=\frac{\omega_mK_0\exp\left(\frac{\Delta h_{ads}M_{adsorbate}}{R_uT_{adsorbent}}\right)P}{\left[1+\left[K_0\exp\left(\frac{\Delta h_{ads}M_{adsorbate}}{R_uT_{adsorbent}}\right)P\right]^n\right]^{1/n}}$, P in mbar, T in K	$\Delta h_{ads}=2760$ *kJ/kg*	$K_0=2.0\times10^{-10}$ mbar^{-} $\omega_m=0.8$ kg/kg $n=1.1$ $R_u=8.314$ J/mol K $M_{adsorbate}=0.018$ kg/mol	[57,66]

Table 4
Constant parameters in the LDF model (Eq. (5)) for adsorbate uptake rate modeling.

LDF model: $\frac{d\omega}{dt}=\frac{15D_s}{R_p^2}(\omega_{eq}-\omega)=\frac{15D_{s0}}{R_p^2}\exp\left(-\frac{E_a}{R_uT_{adsorbent}}\right)(\omega_{eq}-\omega)=k_1\exp(-\frac{k_2}{T_{adsorbent}})(\omega_{eq}-\omega)$

Working pair	Constant parameters					Ref. no.
	D_{s0} (m^2/s)	R_p (m)	E_a (J/mol)	k_1 (1/s)	k_2 (K)	
Zeolite 4 A–water	1.31×10^{-9}	4.0×10^{-6}	5660	1228.12	680.7	[70,71]
Zeolite 13X–water	–	–	7530	4.004×10^{-2}	905.8	[11]
Act. carbon–methanol	–	–	8131	7.35×10^{-3}	978	[72]
Act. carbon–ethanol	$11/15\times1.8\times10^{-12}$	6.5×10^{-6}	14,100	3.046×10^{-6}	1696	[64]
RD silica gel–water	2.54×10^{-4}	1.7×10^{-4}	42,000	1.318×10^{5}	5051.7	[45,57,73]
Silica gel/$CaCl_2$–water	2.54×10^{-4}	1.74×10^{-4}	42,000	1.258×10^{5}	5051.7	[57,73]

known working pairs, namely, zeolite 4A–water, zeolite 13X–water, activated carbon–methanol, activated carbon fibers–ethanol, silica gel–water, and silica gel/$CaCl_2$ (SWS-1)-water. The equilibrium adsorbate uptake by various adsorbent materials and the enthalpy of adsorption of different working pairs are summarized in Table 3.

The information summarized in Table 3 only provides the equilibrium adsorbate uptake by the adsorbent particles whereas in the ACS thermodynamic cycle modeling, adsorbate uptake rate is required because ACS is a dynamic system in which adsorbent particles cannot be fully saturated or dried out during a cycle. Different models for the adsorbate uptake rate have been reported for various boundary conditions and geometries. Ruthven et al. [67,68] provided analytical solutions for the adsorbate uptake rate by zeolite and other microporous materials which, in some cases, are not easy to use. To this end, Glueckauf [69] proposed a simplified model, called linear driving force (LDF) model, for the adsorbate uptake rate of the adsorbent particles. Table 4 shows a summary of the constant parameters in the LDF model, Eq. (5), to calculate the adsorbate uptake rate of different adsorbent particles.

Further information required for thermo-physical properties of working pairs, such as heat capacity, enthalpy of vaporization and saturation pressure, as a function of temperature are tabulated in Table 5.

3.3. Solution method

To solve the set of differential equations simultaneously, an in-hose code is developed using the FORTRAN language. The Runge–

Table 5
Thermo-physical properties of working pairs in ACS modeling.

Material	Thermo-physical properties[a]	Ref. no.
Water	$c_{p,\ liq.\ water} = 5\times10^{-5}T^3 - 0.0465T^2 + 13.476T + 2884.0$ (J/kg K)	Fitted to the data in Ref. [74]
	$c_{p,\ water\ vapor} = 0.0006T^2 - 0.0426T + 1824.1$ (J/kg K)	Fitted to the data in Ref. [74]
	$h_{fg,\ water} = -7.1T^2 + 2620.4T + 2.2866\times10^6$ (J/kg)	Fitted to the data in Ref. [74]
	$P_{sat.,\ water} = \exp(20.5896 - \frac{5098.26}{T})$ (mbar)	[43]
Methanol	$c_{p,\ liq.\ methanol} = 6.3T + 287.8$ (J/kg K)	Fitted to the data in Ref. [75]
	$c_{p,\ methanol\ vapor} = 2.4016T + 657.21$ (J/kg K)	Fitted to the data in Ref. [75]
	$h_{fg,\ methanol} = -10.7T^2 + 5203.4T + 5.5415\times10^5$ (J/kg)	Fitted to the data in Ref. [75]
	$P_{sat.,\ methanol} = \exp(20.84 - \frac{4696.0}{T})$ (mbar)	[43]
Ethanol	$c_{p,\ liq.\ ethanol} = 10.99T - 701.5$ (J/kg K)	Fitted to the data in Ref. [75]
	$c_{p,\ ethanol\ vapor} = 1.635\times10^{-4}T^3 - 0.1391T^2 + 42.3T - 2981.0$ (J/kg K)	Fitted to the data in Ref. [75]
	$h_{fg,\ ethanol} = -6.531T^2 + 2858.0T + 6.526\times10^5$ (J/kg)	Fitted to the data in Ref. [75]
	$P_{sat.,\ ethanol} = \exp(20.272 - \frac{4687.0}{T})$ (mbar)	Fitted to the data in Ref. [75]
Zeolite	$c_{p,\ zeolite} = 836.0$ (J/kg K)	[11]
Activated carbon	$c_{p,\ act.\ carbon} = 920.0$ (J/kg K)	[76]
Silica gel	$c_{p,\ silica\ gel} = 924.0$ (J/kg K)	[57]

[a] Temperature unit in the relationships is in kelvin.

Table 6
Operating conditions in experiments conducted by Grisel et al. [77] and Freni et al. [78].

Reference	Grisel et al. [77]	Freni et al. [78]
System specifications	2-bed silica gel–water ACS	Single-bed silica gel–water ACS
Adsorbent grain size (mm)	0.2–1.0	0.25–0.425
Mass of adsorbent per bed (kg)	8.7	0.437
Metal mass of adsorber bed (kg)	8.4	4.3
Adsorber bed heat transfer surface area, A_{bed}, (m^2)	Not reported	1.66
Adsorber bed heat transfer coefficient, U_{bed}, (W/m^2 K)	Not reported	40.0
Adsorber bed heat transfer conductance, $U_{bed}A_{bed}$, (W/K)	450	66.4
Heating fluid mass flow rate to adsorber bed (kg/s)	0.27 (16.2 L/min water)	0.118 (7.08 L/min water)
Cooling fluid mass flow rate to adsorber bed (kg/s)	0.25 (15.2 L/min water)	0.254 (15.24 L/min water)
Metal mass of condenser (kg)	3.5 (assumed)	3.5
Water mass of condenser (kg)	Not reported	1.5
Condenser heat transfer surface area, A_{cond}, (m^2)	Not reported	0.2719
Condenser heat transfer coefficient, U_{cond}, (W/m^2 K)	Not reported	500.0
Condenser heat transfer conductance, $U_{cond}A_{cond}$, (W/K)	1000	136.0
Coolant water mass flow rate to condenser (kg/s)	0.23 (13.8 L/min water)	0.15 (9.0 L/min water)
Metal mass of evaporator (kg)	3.5 (assumed)	3.5
Water mass of evaporator (kg)	Not reported	1.5
Evaporator heat transfer surface area, A_{evap}, (m^2)	Not reported	0.2719
Evaporator heat transfer coefficient, U_{evap}, (W/m^2 K)	Not reported	500.0
Evaporator heat transfer conductance, $U_{evap}A_{evap}$, (W/K)	1666	136.0
Chilled water mass flow rate to evaporator (kg/s)	0.18 (11.0 L/min water)	0.137 (8.22 L/min water)

Kutta–Fehlberg method (RKF45) is adopted because the differential terms in the governing equations of the ACS fully dynamic modeling are only time-dependent. In the present model, a marching time step of 0.1 s is used and the relative error difference between two consequent iterations at each time step is set at 10^{-9}, respectively. Also, the absolute error difference between the results at the end of two consequent cycles is set at 10^{-3}.

4. Results and discussion

In this section, the accuracy of ACS fully dynamic modeling in prediction of SCP and COP are investigated against the available data in the literature. Next, base-case operating conditions are defined to supply 2 kW of cooling power for a light-duty vehicle under nominal operating conditions. Then, parametric study is conducted to investigate the effects of different parameters on the performance of ACS installed in a light-duty vehicle.

4.1. Comparison of the model against the experimental data

The information required as inputs to the ACS fully dynamic model is summarized in Table 6. These data are extracted from two sets of experimental data reported by Grisel et al. [77] and Freni et al. [78]. It is noteworthy to mention that some of these data have not been reported in Ref. [77,78] and were provided by the corresponding authors in our communications.

Fig. 2 shows the validation of the developed model with the experimental data reported by Grisel et al. [77]. The uncertainty in the data measurements has not been reported by Grisel et al. [77]. Fig. 2a shows the effects of different cycle times on the SCP and COP of ACS. As shown in Fig. 2a, the model followed the same trend as the experimental data with the average relative differences of 10% and 7% for the SCP and COP, respectively. In Fig. 2a, our modeling indicates that the maximum SCP occurs at the cycle time between 10 and 15 min which is in agreement with the experimental data. Fig. 2b and c shows the comparison of the present model with the experimental data for various heating and

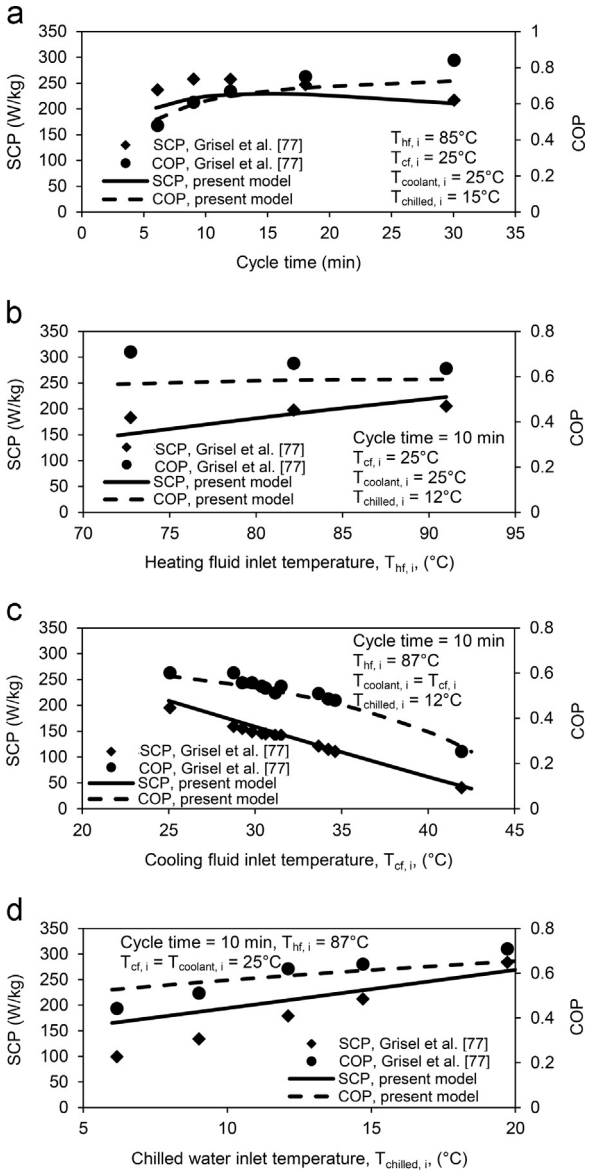

Fig. 2. Comparison between the ACS fully dynamic model and the experimental data reported by Grisel et al. [77]. Variation of SCP and COP vs. (a) cycle time, (b) heating fluid inlet temperature, (c) cooling fluid inlet temperature, and (d) chilled water inlet temperature.

cooling fluids inlet temperatures. The average relative differences for the SCP and COP in Fig. 2b are 10.9% and 12.9%, and for those in Fig. 2c are 6.3% and 5.2%, respectively. Fig. 2d depicts the effects of the chilled water inlet temperature on the SCP and COP of the ACS. It can be seen in Fig. 2d that the model predicts the experimental data with good accuracy.

The comparison between the model and the experimental data reported by Freni et al. [78] is shown in Fig. 3. The uncertainty of 10% was reported in the measurements of the experimental data [78]. In Fig. 3a, the model shows a good agreement with the experimental data. In Fig. 3a, the average relative differences between the predicted SCP and COP with the experimental data are 13% and 3%, respectively. Similar to Fig. 2a, Fig. 3a indicates that the SCP is maximized at the cycle time of 10 min. Fig. 3b and c depicts the variation of SCP and COP for various heating and cooling fluids inlet temperatures. The predicted SCP and COP by the model follow the same trend as the experimental data with a reasonable accuracy.

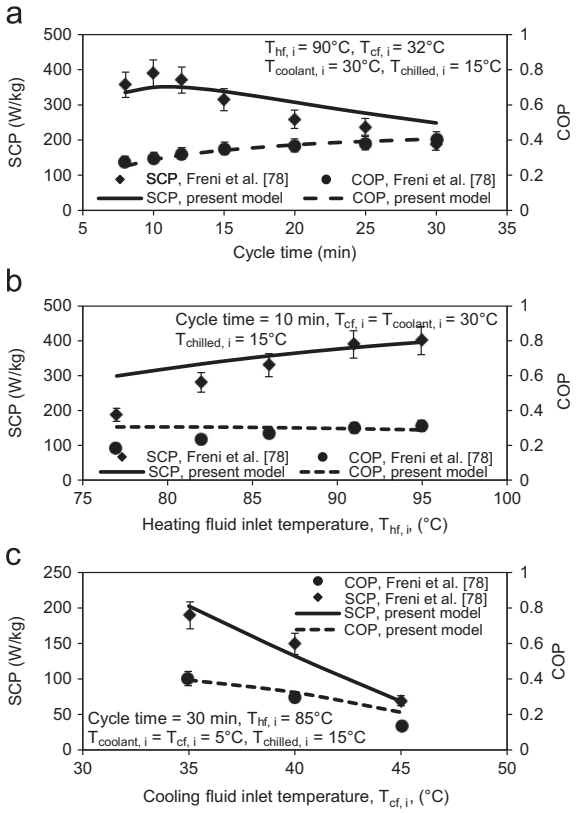

Fig. 3. Comparison between the ACS fully dynamic model and the experimental data reported by Freni et al. [78]. Variation of SCP and COP vs. (a) cycle time, (b) heating fluid inlet temperature, and (c) cooling fluid inlet temperature.

4.2. Base-case model

The ACS designed for a light-duty vehicle A/C system should be able to supply 2 kW of cooling power using the available heat sources in the vehicle, namely, the engine coolant and the exhaust gas of the ICE [2,26]. In the case of using the exhaust gas of the ICE, backpressure along the exhaust line should not increase. For example, the maximum allowable backpressure for diesel engines with powers less than 50, 50–500, and above 500 kW should be 40, 20, and 10 kPa, respectively [79]. To reduce the difficulty of using the exhaust gas of the ICE, the engine coolant is selected as a primary heat source with temperature of 90 °C [26]. The base-case operating conditions as input to our ACS fully dynamic model are summarized in Table 7.

The performance of ACS at the base-case operating conditions is summarized in Table 8. The analysis conducted by De Boer et al. [2] showed that to use solely the engine coolant to regenerate the adsorber beds, the COP of system should be greater than 0.5. As shown in Table 8, the designed ACS for a light-duty vehicle A/C applications has the SCP of 185 W/kg and the COP of 0.55 which is in agreement with De Boer et al. [2] analysis.

4.3. Parametric study

In this section, effects of different salient parameters are investigated on the SCP and COP of ACS. These analyses assist (i) to specify important parameters in the ACS, (ii) to size the system properly, and (iii) to determine the best performance of ACS under different operating conditions.

Fig. 4a shows the effects cycle time on the SCP and COP. It can be seen in Fig. 4 that the SCP is maximized at the cycle time of 10–15 min. By increasing the cycle time from 5 to 10 min, the SCP and

Table 7
Base-case operating conditions applied in the ACS fully dynamic model.

Parameter	Value	Ref. No.
Working pairs	Silica gel–water	–
Mass of adsorbent per bed (kg)	5.0	Calculated
Metal mass of adsorber bed (kg)	5.0	Calculated
Adsorber bed heat transfer surface area, A_{bed}, (m^2)	3.2	Calculated
Adsorber bed heat transfer coefficient, U_{bed}, (W/m^2 K)	100.0	[78]
Heating fluid mass flow rate to adsorber bed (kg/s)	0.2 (12 L/min water)	[26]
Cooling fluid mass flow rate to adsorber bed (kg/s)	0.2 (12 L/min water)	[26]
Metal mass of condenser (kg)	1.5	Calculated
Condenser heat transfer surface area, A_{cond}, (m^2)	0.77	Calculated
Condenser heat transfer coefficient, U_{cond}, (W/m^2 K)	500	[78]
Coolant water mass flow rate to condenser (kg/s)	0.2 (12 L/min water)	[26]
Metal mass of evaporator (kg)	1.5	Calculated
Evaporator heat transfer surface area, A_{evap}, (m^2)	0.77	Calculated
Evaporator heat transfer coefficient, U_{evap}, (W/m^2 K)	1000	[78]
Chilled water mass flow rate to evaporator (kg/s)	0.13 (8 L/min water)	[26]
Heating fluid inlet temperature (°C)	90	[26]
Cooling fluid inlet temperature (°C)	33	[26]
Coolant fluid inlet temperature (°C)	33	[26]
Chilled water inlet temperature (°C)	15	[26]
Cycle time (min)	10	Assumed
Adsorption to desorption time ratio (ADTR)	1.0	Assumed

Table 8
Performance of the proposed ACS for a compact vehicle A/C system under the base-case operating conditions.

Parameter	Value	
Evaporative cooling power, Q_{evap}	2.04 kW	555.16 kJ
Condensation power, Q_{cond}	2.19 kW	588.15 kJ
Total heating power, $Q_{total\ heating}$	10.96 kW	1011.13 kJ
Total cooling power, $Q_{total\ heating}$	10.86 kW	960.35 kJ
COP, Eq. (24)	0.55	
SCP, Eq. (25)	185.0 W/kg	

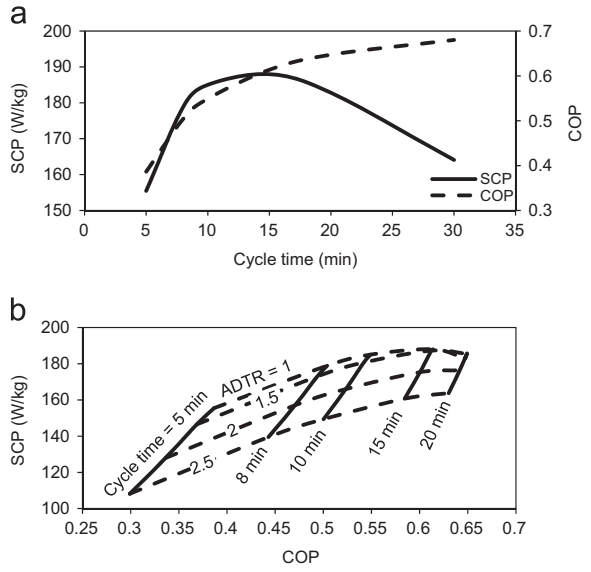

Fig. 4. Variation of SCP and COP as a function of (a) cycle time, and (b) ADTR and cycle time (other parameters are at the base-case operating conditions).

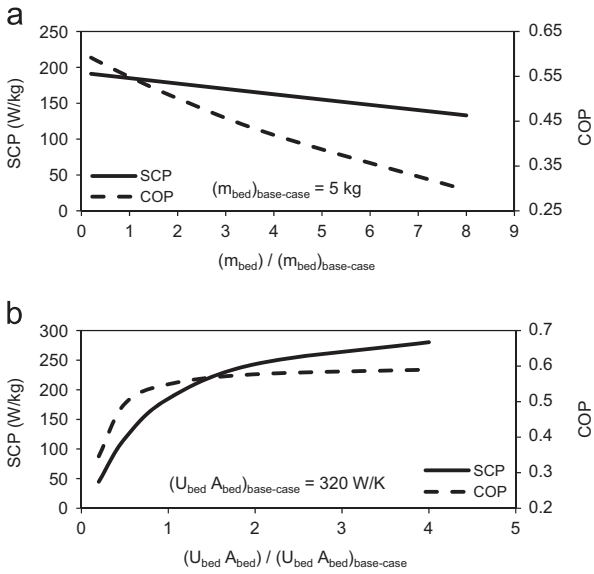

Fig. 5. Variation of SCP and COP as a function of (a) normalized adsorber bed mass, and (b) normalized adsorber bed overall heat transfer conductance (other parameters are at the base-case operating conditions).

COP increase by 19% and 42%, respectively. Whereas, by increasing the cycle time from 10 to 30 min, the SCP reduces from 185 to 164 W/kg (11%) and the COP increase from 0.55 to 0.68 (24%). Fig. 4b depicts the effects of different adsorption to desorption time ratios (ADTR) and cycle times on the SCP and COP. Fig. 4b serves as the characteristic curves of the designed ACS. As shown in Fig. 4b, the highest values for the SCP and COP under a constant cycle time are achieved at the ADTR of one. In addition, Fig. 4b indicates that the maximum SCP and COP are obtained at the cycle times more than 10 min. From Fig. 4b, it can be concluded that the highest SCP and COP of the designed ACS can be accomplished by 2-adsorber bed ACS (ADTR of one) and the cycle times between 10 and 20 min. It should be noted that each ACS has its own characteristic curves and its performance may maximize at different ADTRs such as data reported by Sapienza et al. [80].

Fig. 5 shows the effects of normalized adsorber bed mass and overall heat transfer conductance on the SCP and COP. The adsorber bed mass (dead mass) in vehicles is an important parameter that should be minimized. Fig. 5a indicates that by increasing the normalized adsorber bed mass from 1 to 8, the SCP and COP reduce from 185 to 133 W/kg (28%) and from 0.55 to 0.3 (46%), respectively.

Fig. 5b shows that the SCP is more sensitive than the COP to the overall heat transfer conductance variations. By increasing the normalized adsorber bed overall heat transfer conductance from 1 to 4, the SCP increases by 51%, whereas the COP increases only 7.5%.

Effects of heating fluid inlet temperature on the variations of SCP and COP are shown in Fig. 6a. Although the engine coolant has high temperature, Fig. 6a depicts that the low engine coolant temperature at the cold start-up results in very low SCP and COP. Fig. 6a also indicates that by increasing the heating fluid inlet temperature from 70 to 95 °C, the SCP linearly increases by 127% and the COP increases by 20%, respectively.

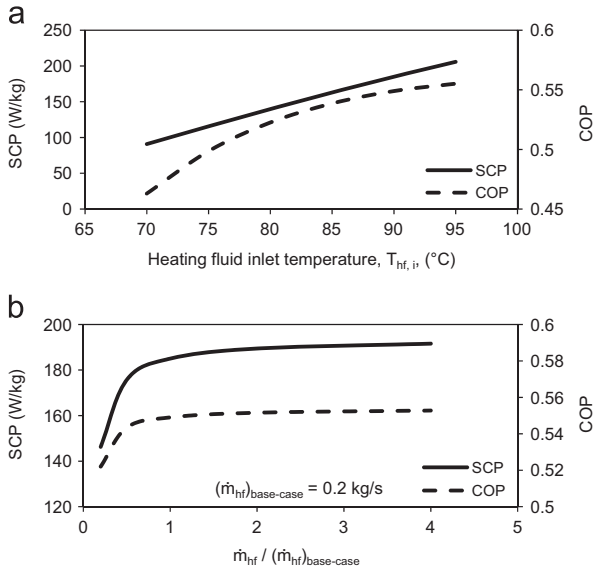

Fig. 6. Variation of SCP and COP as a function of (a) heating fluid inlet temperature, and (b) normalized heating fluid mass flow rate (other parameters are at the base-case operating conditions).

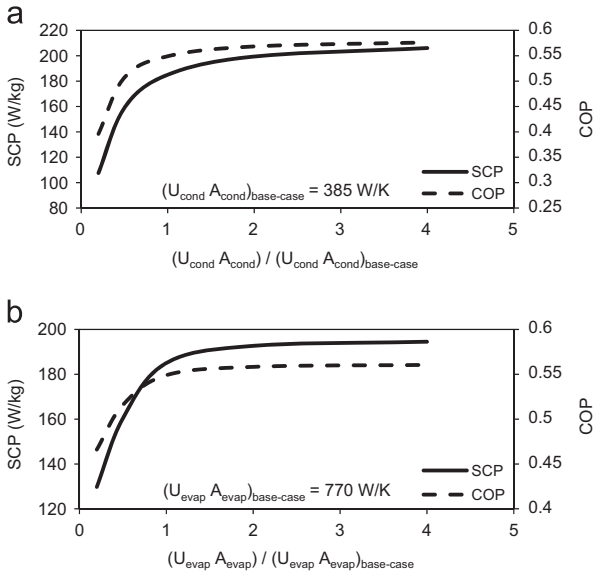

Fig. 8. Variation of SCP and COP as a function of (a) normalized condenser overall heat transfer conductance, and (b) normalized evaporator overall heat transfer conductance (other parameters are at the base-case operating conditions).

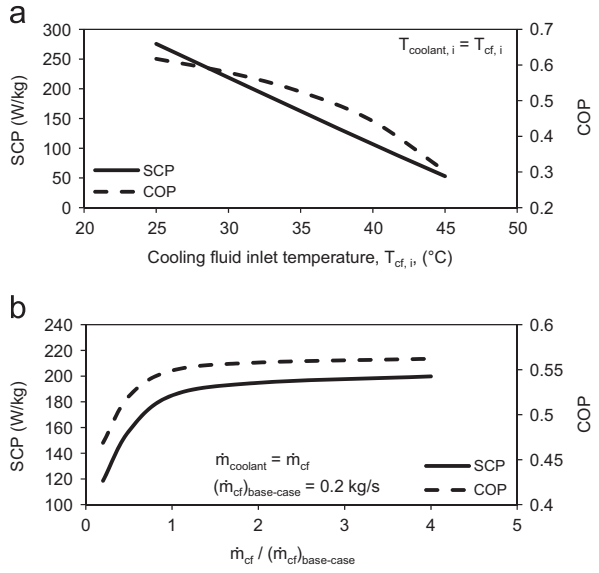

Fig. 7. Variation of SCP and COP as a function of (a) cooling fluid inlet temperature, and (b) normalized cooling fluid mass flow rate (other parameters are at the base-case operating conditions).

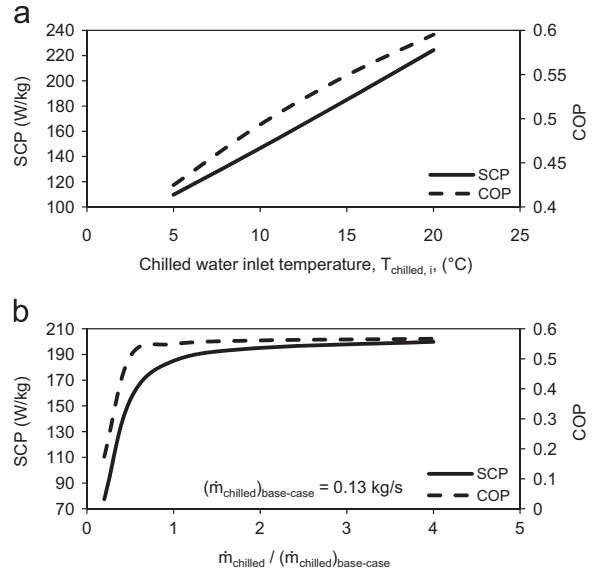

Fig. 9. Variation of SCP and COP as a function of (a) chilled water inlet temperature, and (b) normalized chilled water mass flow rate (other parameters are at the base-case operating conditions).

Fig. 6b shows the effects of normalized heating fluid mass flow rate on the performance of ACS. It can be seen in Fig. 6b that the SCP and COP do not vary significantly by normalized heating fluid mass flow rates greater than 0.75.

Fig. 7 displays the effects of cooling fluid inlet temperature and normalized mass flow rate on the SCP and COP. In a vehicle, the cooling fluid which flows through the adsorber bed and condenser during the adsorption and condensation processes, respectively, comes from an auxiliary radiator which is cooled down by the ambient air [26]. The auxiliary radiator is different from the engine radiator to prevent any interference with the engine cooling process. Therefore, in Fig. 7, it is assumed that the cooling fluid inlet temperature to the adsorber bed and coolant inlet temperature to the condenser have the same temperature and mass flow rate. As shown in Fig. 7a, the SCP linearly decreases from 275.7 to 52.9 W/kg (80%) and the COP reduces from 0.62 to 0.3 (50%) by increasing the cooling fluid inlet temperature from 25 to 45 °C. Comparing Figs. 7 and 6a indicates that for the designed silica gel–water ACS, the SCP and COP are more sensitive to the cooling fluid than the heating fluid inlet temperature. Fig. 7b shows that the SCP and COP remain constant for the normalized cooling fluid mass flow rates greater than one; the SCP and COP increases only 8% and 2.4% by increasing the normalized cooling fluid mass flow rate from 1 to 4.

The importance of sizing or rating of appropriate condensers and evaporators with proper overall heat transfer conductance is depicted in Fig. 8. As shown in Fig. 8a, by increasing the normalized condenser overall heat transfer conductance from 0.2 to 1, the SCP and COP increases by 72% and 38.6%, respectively. However, for the normalized condenser overall heat transfer conductance greater than 1, the SCP and COP do not change considerably.

Fig. 8b shows the effects of the normalized evaporator overall heat transfer conductance on the performance of ACS. It can be seen

in Fig. 8b that the SCP increases from 130 to 185 W/kg (42.6%) and the COP increases from 0.47 to 0.55 (17.8%) by increasing the normalized evaporator overall heat transfer conductance from 0.2 to 1. It should be noted that higher overall heat transfer conductance may result in adding weight to the ACS which should be included in the analysis. Fig. 8 indicates that having a well-designed adsorber bed with proper heat and mass transfer characteristics is not the sole factor in ACS to achieve high SCP and COP.

Fig. 9a demonstrates the effects of chilled water inlet temperature on the SCP and COP. As shown in Fig. 9a, increasing the chilled water inlet temperature from 5 to 20 °C increases the SCP and COP by 105% and 40%, respectively. The cabin temperature thermal comfort temperature range is about 20–23 °C [2]. As a result, the chilled water inlet temperature to the evaporator within the range of 15–20 °C results in achieving the SCP and COP of 185–224 W/kg and 0.55–0.6, respectively.

Fig. 9b depicts the effects of normalized chilled water mass flow rate on the SCP and COP. Fig. 9b indicates that the SCP and COP do not increase effectively for the normalized chilled water mass flow rates greater than one whereas the SCP and COP increases by 139% and 216% by increasing the normalized chilled water mass flow rate from 0.2 to 1.

According to the parametric study, important parameters in the sizing of ACS, which are fixed after building the ACS, are the adsorber bed, condenser and evaporator mass and overall heat transfer conductance (Figs. 5 and 8). Among these parameters, adsorber bed mass has the lowest and adsorber bed overall heat transfer conductance has the highest effects on the SCP. However, the adsorber bed mass should be minimized to reduce the dead mass in vehicles. The cycle time is the other parameter that should be calculated to maximize the SCP under specific operating conditions, see Fig. 4a. Other parameters are the heating and cooling fluids, and chilled water inlet temperatures and mass flow rates (Figs. 6, 7, and 9). According to Figs. 6, 7, and 9, the variable speed pumps are required to adjust the heating and cooling fluids, and chilled water mass flow rates. Although, these mass flow rates do not change the SCP and COP after specific values, their proper adjustments benefit to reach the acceptable SCP and COP with less feeding pump powers. The heating and cooling fluid inlet temperatures to the adsorber bed are fixed by the engine coolant and environment temperatures, respectively. Therefore, these parameters are not under the user control. The only parameter, that significantly changes the SCP and is under the user control, is the chilled water inlet temperature to the evaporator, see Fig. 9a. By adjusting the chilled water mass flow rate, the chilled water inlet temperature to the evaporator can be regulated.

Finally, the parametric study shows that under some operating conditions, the COP of ACS becomes less than 0.5 which indicates the engine coolant may not be sufficient for the regeneration of the adsorber bed during the desorption process. Therefore, depending upon the environmental conditions, a portion of the exhaust gas of the ICE can be used during the desorption process.

5. Conclusion

In this study, the performance of a 2 kW waste-heat driven ACS for light-duty vehicle A/C applications was studied through thermodynamic cycle modeling. The results showed that the SCP and COP of the ACS were maximized for the cycle times between 10 and 15 min and the ADTR of one. In addition, the results indicated that among the adsorber bed, condenser and evaporator, the adsorber bed overall heat transfer conductance and mass have the highest and the lowest effects on the SCP, respectively. Moreover, the results showed that the heating and cooling fluids, coolant and chilled water mass flow rates had not considerable effects on the SCP and COP after specific values. These mass flow rates had to be adjusted in order to reducing the feeding pump powers. Finally, the results showed that for the regeneration of the adsorber beds during the desorption process, the engine coolant was not sufficient and the exhaust gas of the ICE had also to be utilized to achieve the required cooling power under different operating conditions.

Acknowledgment

The authors gratefully acknowledge the financial support of the Natural Sciences and Engineering Research Council of Canada (NSERC) through the Automotive Partnership Canada Grant no. APCPJ 401826-10.

References

[1] Farrington R, Rugh J. Impact of vehicle air-conditioning on fuel economy, tailpipe emissions, and electric vehicle range. In: Proceeding of the earth technology forum. Washington, DC; 2000.
[2] De Boer R, Smeding SF. Thermally operated mobile air-conditioning system: development and test of a laboratory prototype. In: Proceeding of the international sorption heat pump conference. Seoul, Korea; 2008.
[3] Suzuki M. Application of adsorption cooling systems to automobiles. Heat Recover Syst CHP 1993;13:335–40.
[4] Abdullah MO, Tan IAW, Lim LS. Automobile adsorption air-conditioning system using oil palm biomass-based activated carbon: a review. Renew Sustain Energy Rev 2011;15:2061–72. http://dx.doi.org/10.1016/j.rser.2011.01.012.
[5] Demir H, Mobedi M, Ülkü S. A review on adsorption heat pump: problems and solutions. Renew Sustain Energy Rev 2008;12:2381–403. http://dx.doi.org/10.1016/j.rser.2007.06.005.
[6] Hulse GE. Freight car refrigeration by an adsorption system employing silica gel. Refrig Eng 1929;17:41–54.
[7] Aceves SM. An analytical comparison of adsorption and vapor compression air conditioners for electric vehicle applications. J Energy Resour Technol 1996;118:16–21.
[8] Hendricks TJ. Vehicle transient air conditioning analysis: model development and system optimization investigations. National Renewable Energy Laboratory, NREL/TP, 540-30715; 2001.
[9] Hendricks TJ. Optimization of vehicle air conditioning systems using transient air conditioning performance analysis. In: SAE conference proceedings; 2001.
[10] Hendricks TJ. Multi-variable optimization of electrically-driven vehicle air conditioning systems using transient performance analysis. In: Proceedings of the SAE vehicle thermal management system; 2003.
[11] Zhang LZ, Wang L. Performance estimation of an adsorption cooling system for automobile waste heat recovery. Appl Therm Eng 1997;17:1127–39.
[12] Zhang LZ, Wang L. Momentum and heat transfer in the adsorbent of a waste-heat adsorption cooling system. Energy 1999;24:605–24. http://dx.doi.org/10.1016/S0360-5442(99)00018-3.
[13] Zhang LZ, Wang L. Effects of coupled heat and mass transfers in adsorbent on the performance of a waste heat adsorption cooling unit. Appl Therm Eng 1999;19:195–215.
[14] Zhang LZ. Design and testing of an automobile waste heat adsorption cooling system. Appl Therm Eng 2000;20:103–14. http://dx.doi.org/10.1016/S1359-4311(99)00009-5.
[15] Zhang LZ. A three-dimensional non-equilibrium model for an intermittent adsorption cooling system. Sol Energy 2000;69:27–35. http://dx.doi.org/10.1016/S0038-092X(00)00010-4.
[16] Jiangzhou S, Wang RZ, Lu YZ, Xu YX, Wu JY. Experimental investigations on adsorption air-conditioner used in internal-combustion locomotive driver-cabin. Appl Therm Eng 2002;22:1153–62. http://dx.doi.org/10.1016/S1359-4311(02)00036-4.
[17] Lu YZ, Wang RZ, Jianzhou S, Zhang M, Xu Y, Wu J. Performance of a diesel locomotive waste-heat-powered adsorption air conditioning system. Adsorption 2004;10:57–68.
[18] Christy C, Toossi R. Adsorption air-conditioning for containerships and vehicles; 2004.
[19] Lambert MA, Jones BJ. Automotive adsorption air conditioner powered by exhaust heat. Part 1: conceptual and embodiment design. Proc Inst Mech Eng Part D J Automob Eng 2006;220:959–72. http://dx.doi.org/10.1243/09544070JAUTO221.
[20] Lambert MA, Jones BJ. Automotive adsorption air conditioner powered by exhaust heat. Part 2: detailed design and analysis. Proc Inst Mech Eng Part D J Automob Eng 2006;220:973–89. http://dx.doi.org/10.1243/09544070JAUTO222.
[21] Wang K, Wu JY, Wang RZ, Wang LW. Composite adsorbent of $CaCl_2$ and expanded graphite for adsorption ice maker on fishing boats. Int J Refrig 2006;29:199–210. http://dx.doi.org/10.1016/j.ijrefrig.2005.06.004.

[22] Wang LW, Wang RZ, Lu ZS, Xu YX, Wu JY. Split heat pipe type compound adsorption ice making test unit for fishing boats. Int J Refrig 2006;29:456–68. http://dx.doi.org/10.1016/j.ijrefrig.2005.08.007.
[23] Lu ZS, Wang RZ, Li TX, Wang LW, Chen CJ. Experimental investigation of a novel multifunction heat pipe solid sorption icemaker for fishing boats using $CaCl_2$/activated carbon compound – ammonia. Int J Refrig 2007;30:76–85. http://dx.doi.org/10.1016/j.ijrefrig.2006.07.001.
[24] Wang K, Wu JY, Xia ZZ, Li SL, Wang RZ. Design and performance prediction of a novel double heat pipes type adsorption chiller for fishing boats. Renew Energy 2008;33:780–90. http://dx.doi.org/10.1016/j.renene.2007.04.023.
[25] Wang LW, Wang RZ, Xia ZZ, Wu JY. Studies on heat pipe type adsorption ice maker for fishing boats. Int J Refrig 2008;31:989–97. http://dx.doi.org/10.1016/j.ijrefrig.2008.01.002.
[26] De Boer R, Smeding SF, Mola S. Silicagel–water adsorption cooling prototype system for mobile air conditioning. In: Proceedings of the heat powered cycles conference. Berlin, Germany; 2009.
[27] Narayanan S, Yang S, Kim H, Wang EN. Optimization of adsorption processes for climate control and thermal energy storage. Int J Heat Mass Transf 2014;77:288–300. http://dx.doi.org/10.1016/j.ijheatmasstransfer.2014.05.022.
[28] Narayanan S, Li X, Yang S, McKay I, Kim H, Wang EN. Design and optimization of high performance adsorption-based thermal battery. In: Proceedings of the ASME 2013 heat transfer summer conference. Minneapolis, MN, USA; 2013. p. 1–10.
[29] Sharafian A, Bahrami M. A quasi steady state model for adsorption cooling systems: Automotive applications. In: Proceedings of the ASME 2012 6th international conference on energy sustainability and 10th fuel cell science, engineering and technology conference. San Diego, CA, USA; 2012.
[30] Yong L, Sumathy K. Review of mathematical investigation on the closed adsorption heat pump and cooling systems. Renew Sustain Energy Rev 2002;6:305–38. http://dx.doi.org/10.1016/S1364-0321(02)00010-2.
[31] Miltkau T, Dawoud B. Dynamic modeling of the combined heat and mass transfer during the adsorption/desorption of water vapor into/from a zeolite layer of an adsorption heat pump. Int J Therm Sci 2002;41:753–62. http://dx.doi.org/10.1016/S1290-0729(02)01369-8.
[32] Marletta L, Maggio G, Freni A, Ingrasciotta M, Restuccia G. A non-uniform temperature non-uniform pressure dynamic model of heat and mass transfer in compact adsorbent beds. Int J Heat Mass Transf 2002;45:3321–30. http://dx.doi.org/10.1016/S0017-9310(02)00045-5.
[33] Leong KC, Liu Y. Numerical study of a combined heat and mass recovery adsorption cooling cycle. Int J Heat Mass Transf 2004;47:4761–70. http://dx.doi.org/10.1016/j.ijheatmasstransfer.2004.05.030.
[34] Leong KC, Liu Y. Numerical modeling of combined heat and mass transfer in the adsorbent bed of a zeolite/water cooling system. Appl Therm Eng 2004;24:2359–74. http://dx.doi.org/10.1016/j.applthermaleng.2004.02.014.
[35] Chua HT, Ng KC, Wang W, Yap C, Wang XL. Transient modeling of a two-bed silica gel–water adsorption chiller. Int J Heat Mass Transf 2004;47:659–69. http://dx.doi.org/10.1016/j.ijheatmasstransfer.2003.08.010.
[36] Maggio G, Freni A, Restuccia G. A dynamic model of heat and mass transfer in a double-bed adsorption machine with internal heat recovery. Int J Refrig 2006;29:589–600. http://dx.doi.org/10.1016/j.ijrefrig.2005.10.005.
[37] Liu Y, Leong KC. Numerical modeling of a zeolite/water adsorption cooling system with non-constant condensing pressure. Int Commun Heat Mass Transf 2008;35:618–22. http://dx.doi.org/10.1016/j.icheatmasstransfer.2007.12.004.
[38] Hu P, Yao J, Chen Z. Analysis for composite zeolite/foam aluminum–water mass recovery adsorption refrigeration system driven by engine exhaust heat. Energy Convers Manag 2009;50:255–61. http://dx.doi.org/10.1016/j.enconman.2008.09.022.
[39] Chen CJ, Wang RZ, Xia ZZ, Kiplagat JK. Study on a silica gel–water adsorption chiller integrated with a closed wet cooling tower. Int J Therm Sci 2010;49:611–20. http://dx.doi.org/10.1016/j.ijthermalsci.2009.09.009.
[40] Riffel DB, Wittstadt U, Schmidt FP, Núñez T, Belo Fa, Leite APF, et al. Transient modeling of an adsorber using finned-tube heat exchanger. Int J Heat Mass Transf 2010;53:1473–82. http://dx.doi.org/10.1016/j.ijheatmasstransfer.2009.12.001.
[41] Ge TS, Dai YJ, Wang RZ. Performance study of silica gel coated fin-tube heat exchanger cooling system based on a developed mathematical model. Energy Convers Manag 2011;52:2329–38. http://dx.doi.org/10.1016/j.enconman.2010.12.047.
[42] Solmuş İ, Rees DAS, Yamalı C, Baker D, Kaftanoğlu B. Numerical investigation of coupled heat and mass transfer inside the adsorbent bed of an adsorption cooling unit. Int J Refrig 2012;35:652–62. http://dx.doi.org/10.1016/j.ijrefrig.2011.12.006.
[43] Cacciola G, Restuccia G. Reversible adsorption heat pump: a thermodynamic model. Int J Refrig 1995;18:100–6. http://dx.doi.org/10.1016/0140-7007(94)00005-I.
[44] Hajji A, Khalloufi S. Theoretical and experimental investigation of a constant-pressure adsorption process. Int J Heat Mass Transf 1995;38:3349–58. http://dx.doi.org/10.1016/0017-9310(95)00102-F.
[45] Sokada A, Suzuki M. Fundamental study on solar powered adsorption. J Chem Eng Jpn 1984;17:52–7.
[46] Sakoda A, Suzuki M. Simultaneous transport of heat and adsorbate in closed type adsorption cooling system utilizing solar heat. J Sol Energy Eng 1986;108:239–45.
[47] Tiansuwan J, Hirunlabh J. Mathematical model of an activated carbon–ethanol refrigerator. Thammasat Int J Sci Technol 1998;3:66–71.
[48] Saha BB, Boelman EC, Kashiwagi T. Computational analysis of an advanced adsorption-refrigeration cycle. Energy 1995;20:983–94.
[49] Saha BB, Akisawa A, Kashiwagi T. Silica gel water advanced adsorption refrigeration cycle. Energy 1997;22:437–47.
[50] Wu JY, Wang RZ, Xu YX. Dynamic simulation and experiments of a heat regenerative adsorption heat pump. Energy Convers Manag 2000;41:1007–18. http://dx.doi.org/10.1016/S0196-8904(99)00161-2.
[51] Chua HT, Ng KC, Malek A, Kashiwagi T, Akisawa A, Saha BB. Modeling the performance of two-bed, silica gel–water adsorption chillers. Int J Refrig 1999;22:194–204.
[52] Wang DC, Xia ZZ, Wu JY, Wang RZ, Zhai H, Dou WD. Study of a novel silica gel–water adsorption chiller. Part I. Design and performance prediction. Int J Refrig 2005;28:1073–83. http://dx.doi.org/10.1016/j.ijrefrig.2005.03.001.
[53] Wang DC, Wu JY, Xia ZZ, Zhai H, Wang RZ, Dou WD. Study of a novel silica gel–water adsorption chiller. Part II. Experimental study. Int J Refrig 2005;28:1084–91. http://dx.doi.org/10.1016/j.ijrefrig.2005.03.002.
[54] Khan MZI, Alam KCa, Saha BB, Hamamoto Y. Akisawa a., Kashiwagi T. Parametric study of a two-stage adsorption chiller using re-heat—The effect of overall thermal conductance and adsorbent mass on system performance. Int J Therm Sci 2006;45:511–9. http://dx.doi.org/10.1016/j.ijthermalsci.2005.08.003.
[55] Wang X, Chua HT. Two bed silica gel–water adsorption chillers: an effectual lumped parameter model. Int J Refrig 2007;30:1417–26. http://dx.doi.org/10.1016/j.ijrefrig.2007.03.010.
[56] Wang X, Chua HT. A comparative evaluation of two different heat-recovery schemes as applied to a two-bed adsorption chiller. Int J Heat Mass Transf 2007;50:433–43. http://dx.doi.org/10.1016/j.ijheatmasstransfer.2006.08.003.
[57] Saha BB, Chakraborty A, Koyama S, Aristov YI. A new generation cooling device employing $CaCl_2$-in-silica gel–water system. Int J Heat Mass Transf 2009;52:516–24. http://dx.doi.org/10.1016/j.ijheatmasstransfer.2008.06.018.
[58] Miyazaki T, Akisawa A, Saha BB, El-Sharkawy II, Chakraborty A. A new cycle time allocation for enhancing the performance of two-bed adsorption chillers. Int J Refrig 2009;32:846–53. http://dx.doi.org/10.1016/j.ijrefrig.2008.12.002.
[59] Verde M, Cortés L, Corberán JM, Sapienza A, Vasta S, Restuccia G. Modelling of an adsorption system driven by engine waste heat for truck cabin A/C. Performance estimation for a standard driving cycle. Appl Therm Eng 2010;30:1511–22. http://dx.doi.org/10.1016/j.applthermaleng.2010.04.005.
[60] Verde M, Corberan JM, de Boer R, Smeding S. Modelling of a waste heat driven silica gel/water adsorption cooling system comparison with experimental results. In: Proceedings of the ISHPC conference. Padua, Italy; 2011. p. 7–8.
[61] Gong LX, Wang RZ, Xia ZZ, Chen CJ. Design and performance prediction of a new generation adsorption chiller using composite adsorbent. Energy Convers Manag 2011;52:2345–50. http://dx.doi.org/10.1016/j.enconman.2010.12.036.
[62] Rahman A, Ueda Y, Akisawa A, Miyazaki T, Saha B. Design and performance of an innovative four-bed, three-stage adsorption cycle. Energies 2013;6:1365–84. http://dx.doi.org/10.3390/en6031365.
[63] Restuccia G, Freni A, Vasta S, Aristov YI. Selective water sorbent for solid sorption chiller: experimental results and modelling. Int J Refrig 2004;27:284–93. http://dx.doi.org/10.1016/j.ijrefrig.2003.09.003.
[64] Saha BB, El-Sharkawy II, Chakraborty A, Koyama S. Study on an activated carbon fiber–ethanol adsorption chiller: Part I – system description and modelling. Int J Refrig 2007;30:86–95. http://dx.doi.org/10.1016/j.ijrefrig.2006.08.004.
[65] Chua HT, Ng KC, Chakraborty A, Oo NM, Othman MA. Adsorption characteristics of silica gel+water systems. J Chem Eng Data 2002;47:1177–81. http://dx.doi.org/10.1021/je0255067.
[66] Aristov YI, Tokarev MM, Cacciola G, Restuccia G. Selective water sorbents for multiple applications, 1. $CaCl_2$ confined in mesopores of silica gel: sorption properties. React Kinet Catal Lett 1996;59:325–33.
[67] Ruthven DM. Principles of adsorption and desorption processes. United States of America: John Wiley & Sons, Inc.; 1984.
[68] Karger J, Ruthven DM. Diffusion in zeolites and other microporous solids. United States of America: Wiley & Sons, Inc.; 1992.
[69] Glueckauf E. Theory of chromatography. Part 10 – formulæ for diffusion into spheres and their application to chromatography. Trans Faraday Soc 1955;51:1540–51.
[70] Kärger J, Pfeifer H, Rosemann M, Feokistova NN, Ž danov SP. Intracrystalline self-diffusion of water and short-chain-length paraffins in A-type zeolites. Zeolites 1989;9:247–9.
[71] Tatlıer M, Tantekin-Ersolmaz B, Erdem-Şenatalar A. A novel approach to enhance heat and mass transfer in adsorption heat pumps using the zeolite–water pair. Microporous Mesoporous Mater 1999;27:1–10. http://dx.doi.org/10.1016/S1387-1811(98)00174-7.
[72] Passos EF, Escobedo JF, Meunier F. Simulation of an intermittent adsorptive solar cooling system. Sol Energy 1989;42:103–11.
[73] Aristov YI, Glaznev IS, Freni A, Restuccia G. Kinetics of water sorption on SWS-1 L (calcium chloride confined to mesoporous silica gel): influence of grain size and temperature. Chem Eng Sci 2006;61:1453–8. http://dx.doi.org/10.1016/j.ces.2005.08.033.
[74] Cengel YA, Boles MA. Thermodynamcis: an engineering approach. New York: McGraw-Hill; 2006.
[75] Green DW, Perry RH. Perry's chemical engineers' handbook. 8th editionMcGraw-Hill Professional; 2007.
[76] Zhao Y, Hu E, Blazewicz A. Dynamic modelling of an activated carbon–methanol adsorption refrigeration tube with considerations of interfacial convection and transient pressure process. Appl Energy 2012;95:276–84. http://dx.doi.org/10.1016/j.apenergy.2012.02.050.

[77] Grisel RJH, Smeding SF, de Boer R. Waste heat driven silica gel/water adsorption cooling in trigeneration. Appl Therm Eng 2010;30:1039–46. http://dx.doi.org/10.1016/j.applthermaleng.2010.01.020.
[78] Freni A, Sapienza A, Glaznev IS, Aristov YI, Restuccia G. Experimental testing of a lab-scale adsorption chiller using a novel selective water sorbent "silica modified by calcium nitrate". Int J Refrig 2012;35:518–24. http://dx.doi.org/10.1016/j.ijrefrig.2010.05.015.
[79] Mayer A. Number-based emission limits, VERT-DPF verification procedure and experience with 8000 retrofits. Switzerland; 2004.
[80] Sapienza A, Santamaria S, Frazzica A, Freni A. Influence of the management strategy and operating conditions on the performance of an adsorption chiller. Energy 2011;36:5532–8. http://dx.doi.org/10.1016/j.energy.2011.07.020.